# $4d^{-1}$ multiplet structure of rare-earth atoms studied by photoelectron-ion coincidence spectroscopy

Ch. Gerth, A. G. Kochur,* M. Groen, T. Luhmann, M. Richter, and P. Zimmermann
*Institut für Atomare und Analytische Physik, Technische Universität Berlin, 10623 Berlin, Hardenbergstrasse 36, Germany*
(Received 30 October 1997)

The $4d$ photoelectron spectra of atomic lanthanides Ce, Pr, Nd, Sm, and Eu have been measured using synchrotron radiation. The multiplet structure of the $4d^{-1}$ hole states has been investigated by applying the electron-ion coincidence technique in the form of final ion-charge resolving electron (FIRE) spectroscopy. FIRE spectroscopy is a spin-sensitive method for the study of $4d^{-1}$ decay processes. Photoelectron spectra have been calculated in the one-configuration approximation for the rare-earth atoms from Ce to Gd and FIRE spectra have been calculated for Ce, Pr, Nd, Sm, and Eu. Comparing theoretical and experimental results, we discuss the trend of the development of the $4d^{-1}$ multiplet structure from Ce to Gd. [S1050-2947(98)01805-8]

PACS number(s): 32.80.Fb

## I. INTRODUCTION

Recently, a new type of electron spectroscopy has been developed that allows photoelectron spectra of free atoms to be split into partial contributions corresponding to the formation of ions of specific charges [1–4]. We called this technique final ion-charge resolving electron (FIRE) spectroscopy. Luhmann *et al.* [2] have applied this technique to study the structure of the $4d^{-1}$ multiplets in Eu and Sm. A strong dependence of the FIRE spectra on the ion charge has been reported. Specifically, the low ionization energy part of the $4d$ FIRE(2+) spectra was found to be strongly suppressed. It was suggested in Ref. [2] that such behavior of the photoelectron-ion coincidence spectra might be explained by (otherwise very intense) forbidden super-Coster-Kronig $4d-4f4f$ transitions for the high-spin components of the $4d^{-1}$ multiplets leading to doubly charged ions.

The first theoretical description of the $4d$ FIRE spectra of Eu was given by Kochur *et al.* [5], who combined multiplet structure calculations with calculations of ion yields in the configuration-average approximation. It was pointed out that the $4d$ FIRE spectra of rare earths should be sensitive to the localization of high-spin states within the $4d^{-1}$ multiplets.

Systematic calculations of the structure of the $4d^{-1}$ multiplets in the rare-earth elements in the one-configuration approximation were performed by Demekhin *et al.* [6]. They pointed out that in the one-configuration approximation reasonable agreement with experimental results can only be obtained by accounting for many-electron correlations. This can approximately be achieved by scaling the integrals of the $4f-4f$ and $4d-4f$ interactions. The calculations of Ref. [6] as well as calculations on Eu [5] and Gd [7,8] showed that the $4d$ spectra of the rare-earth elements extend over an energy range of about 30 eV and can be roughly divided into an intense low ionization energy region and a less intense high ionization energy region. The low ionization energy part of the $4d$ photoelectron spectra of free rare-earth atoms has been the subject of a number of experimental studies (see [9,10] and references therein). Contradictory assignments of the low ionization energy region were given by different authors. Ogasawara *et al.* [11] performed calculations on the $4d$ photoelectron spectra of rare earths (Sm to Lu) and discussed the role of forbidden super-Coster-Kronig $4d-4f4f$ transitions in the lifetime broadening of the $4d^{-1}$ multiplet components. Based on these calculations, they assigned the whole low ionization energy region to high-spin states.

FIRE spectroscopy is a powerful tool for distinguishing between high-spin and low-spin states of the $4d^{-1}$ multiplets in rare-earth atoms. For example, calculations [5] and measurements with FIRE spectroscopy [2] showed that only the lowest ionization energy peak in the $4d$ photoelectron spectrum of Eu represents predominantly high-spin $^9D$ states, while the neighboring secondary peak reflects low-spin $^7D$ states arising from the coupling of the $4d$ vacancy with $4f^7(^6L)$ states. Similar assignments were given by van der Laan *et al.* [7], who studied the magnetic circular dichroism in the $4d$ photoemission of metallic Gd, and later on by Lademan *et al.* [8], who measured and calculated spin-resolved Gd $4d$ photoelectron spectra.

Dichroism measurements on magnetized solid state samples and spin-resolved photoelectron spectroscopy are other examples of spin-sensitive methods for the study of the composition of multiplet states. First experimental data on the dichroism in the $3p$ photoelectron spectra of free Cr atoms were recently reported by von dem Borne *et al.* [12]. In that type of experiment, the alignment or orientation of atoms is obtained by laser pumping using linearly or circularly polarized light. The spin-sensitivity of FIRE spectroscopy is not induced by an external influence, such as magnetization or laser pumping, but is an intrinsic property of the decay processes following the creation of an inner-shell vacancy.

In this work we present the $4d$ photoelectron and FIRE spectra of Ce, Pr, Nd, Sm, and Eu as well as calculations of spectra for the whole series from Ce to Gd. We discuss the structure of the $4d^{-1}$ multiplets, focusing on the trends of the high-spin state distributions. The question of the high-

*Permanent address: Rostov State University of Transport Communication, Narodnogo Opolcheniya Square 2, Rostov-na-Donu 344038, Russia.

 

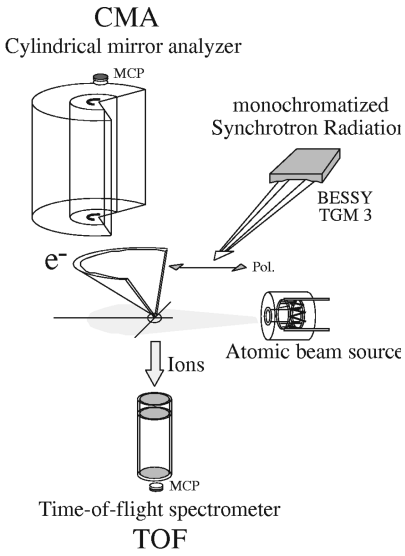


FIG. 1. Scheme of the main parts of the experimental setup showing the cylindrical mirror analyzer (CMA), the time-of-flight spectrometer (TOF), the atomic beam source, and the synchrotron radiation beam.

spin state distribution within the $4d^{-1}$ multiplets is resolved with the help of FIRE spectroscopy.

## II. EXPERIMENT

The experiments were performed at the electron storage ring BESSY in Berlin. A scheme showing the main parts of the experimental setup is depicted in Fig. 1. Monochromatized synchrotron radiation, provided by the toroidal grating monochromater TGM3 with a resolution power of about 120, crosses a beam of rare-earth atoms produced by the atomic-beam technique [13]. In the case of Sm and Eu, free atoms were produced by thermal evaporation in a resistively heated crucible, while the necessary temperatures for the elements Ce, Pr, and Nd were achieved by electron impact heating. The temperatures and the corresponding thermal population of initial states for these elements are listed in Table I. For the evaporation of Ce and Nd, we used an $Al_2O_3$ crucible within a molybdenum crucible to avoid direct contact between the metals being investigated and the molybdenum. Electrons emitted in the photoionization process are analyzed according to their kinetic energy $\epsilon$ by a 180° cylindrical mirror analyzer (CMA). The CMA has an angular acceptance of 1.2% of $4\pi$ and an energy resolution of $\Delta E/E = 1.00(7)\%$. Only electrons emitted close to the magic angle ($54.7° \pm 1.7°$ with respect to the spectrometer axis) are accepted by the CMA. A photoelectron spectrum $\mathrm{EDC}_{h\nu}(\epsilon)$ (energy distribution curve) is recorded while scanning the kinetic energy $\epsilon$ at fixed photon energy $h\nu$. Photoions are separated according to their mass to charge ratio $m/q$ using a time-of-flight (TOF) spectrometer of the Wiley-McLaren type [14]. By application of an electrical extraction pulse ($-40$ V, $4\mu$s), the photoions are accelerated towards the entrance aperture of the TOF. After a second post-acceleration stage ($-60$ V), the ions reach the field-free drift tube. Finally, the ions are accelerated onto the detector by applying a voltage of $-3$ kV. The TOF spectrometer and the CMA are equipped with microchannel plates (MCP) for particle detection. For the TOF measurements a time-to-digital multistop counter (TDC) is used. The TOF spectra are corrected for the ion detection efficiency of the MCP detector for different charge states [4].

TABLE I. Temperatures of atomic beams ($T$), energy separations ($\Delta E_{L_0S_0J_0}$), and thermal population of the initial $L_0S_0J_0$ states ($\mathcal{W}_{L_0S_0J_0}$).

| Element | $T$ (K) | $^{2S_0+1}L_{0J_0}$ | $\Delta E_{L_0S_0J_0}$ (meV)[a] | $\mathcal{W}_{L_0S_0J_0}$ |
|---|---|---|---|---|
| Ce($4f^15d^1$) | 1850 | $^1G_4$ | 0 | 0.38 |
| | | $^3F_2$ | 28 | 0.18 |
| | | $^3H_4$ | 159 | 0.14 |
| | | $^3G_3$ | 172 | 0.10 |
| | | $^3F_3$ | 206 | 0.08 |
| Pr($4f^3$) | 1750 | $^4I_{9/2}$ | 0 | 0.63 |
| | | $^4I_{11/2}$ | 171 | 0.25 |
| | | $^4I_{13/2}$ | 353 | 0.09 |
| Nd($4f^4$) | 1600 | $^5I_4$ | 0 | 0.59 |
| | | $^5I_5$ | 140 | 0.27 |
| | | $^5I_6$ | 293 | 0.10 |
| Sm($4f^6$) | 1000 | $^7F_0$ | 0 | 0.17 |
| | | $^7F_1$ | 36 | 0.34 |
| | | $^7F_2$ | 101 | 0.27 |
| | | $^7F_3$ | 185 | 0.15 |
| Eu($4f^7$) | 900 | $^8S_{7/2}$ | 0 | 1.00 |

[a]Optical data from Ref. [24].

A correlation analysis of electron-ion pairs resulting from one photoionization process is achieved by combining photoelectron and photoion spectroscopy. An electron detected with the selected kinetic energy starts a TOF measurement by triggering the electrical extraction pulse, which accelerates the corresponding coincident ion into the TOF spectrometer. Usually not only this coincident ion is extracted by the electrical pulse but also ions created in other ionization processes. Therefore, the resulting coincidence spectrum contains both true and random signals. These random coincidences are measured separately in a reference spectrum, which is a normal ion TOF spectrum where the electrical extraction pulse is triggered by a pulse generator. Coincidence and reference spectra are recorded under almost the same experimental conditions by switching between the two modes every five seconds. The spectrum of true coincidences is deduced from the coincidence and reference spectra with the help of an evaluation procedure that is described in detail in Ref. [3]. With this method we were able to achieve high coincidence counting rates. Reduction of the photon flux is another way to avoid random coincidences in the coincidence spectrum, but this drastically increases the data accumulation time. After normalization, the spectrum of true coincidences provides the correlation probabilities $p_{h\nu}(\epsilon, n+)$ for the production of $n+$ final ion-charge states upon emission of electrons of selected kinetic energy $\epsilon$. By multiplying the electron spectrum $\mathrm{EDC}_{h\nu}(\epsilon)$ by the correlation probabilities $p_{h\nu}(\epsilon, n+)$ for fixed $n+$ and $h\nu$, one obtains the final ion-charge resolved electron FIRE($n+$) spectrum:

$$\mathrm{EDC}^{n+}_{h\nu}(\epsilon) = p_{h\nu}(\epsilon, n+)\,\mathrm{EDC}_{h\nu}(\epsilon). \qquad (1)$$

The FIRE($n+$) spectrum represents the contribution of those photoionization processes to the photoelectron spectrum which end up in an $n+$ final ion-charge state.

A detailed description of the experimental setup and the electron-ion coincidence technique for energy analyzed electrons is given in Ref. [4]. In that paper, the $4d$ photoionization of Xe was chosen to demonstrate the coincidence method in its extended form of FIRE spectroscopy.

## III. THEORY

### A. Calculation of photoelectron spectra and FIRE spectra

Since the structure of the $4d^{-1}$ multiplets in rare-earth atoms is known to be determined predominantly by the $4d-4f$ and $4f-4f$ electrostatic interaction and the $4d$ spin-orbit interaction [5–7,11], we employ the one-configuration approximation and neglect the $6s-5d$ configuration mixing. The ground state configurations of the atoms under study are taken to be $4f^15d^16s^2$(Ce), $4f^36s^2$ (Pr), $4f^46s^2$ (Nd), $4f^56s^2$ (Pm), $4f^66s^2$ (Sm), $4f^76s^2$ (Eu), and $4f^75d^16s^2$ (Gd).

The wave functions of the $4d^{-1}$ core-holes are calculated in the form

$$|EJ\rangle=\sum_i \langle 4d^9 4f^n\gamma_i,L_i,S_i,J|EJ\rangle|4d^9 4f^n\gamma_i,L_i,S_i,J\rangle. \tag{2}$$

The self-energies $E$ and the decomposition coefficients $\langle 4d^9 4f^n\gamma_i,L_i,S_i,J|EJ\rangle$ are obtained by numerical diagonalization of matrices on the basis sets $\{|4d^9 4f^n\gamma_i,L_i,S_i,J\rangle\}$, where $\gamma_i$ denotes additional quantum numbers. In the case of Ce and Gd, $4f^n$ has to be replaced by $4f^n5d$. The matrix elements of the operators for the electron-electron and spin-orbit interactions are calculated by the methods described in Ref. [15]. To account for many-electron corrections, all the electron-electron interaction Slater integrals calculated in the Hartree-Fock-Pauli approximation were scaled by a factor of 0.7 [6,16]. For Nd to Gd, only the largest and the second-largest multiplicity terms of the $4f^n$ subshells were included in the basis sets. The inclusion of additional terms did not result in any noticeable changes in the calculated photoelectron spectra.

The final state wave functions for the photoionization process

$$A(L_0S_0J_0)+h\nu\rightarrow A(4d^{-1}EJ)+\epsilon\ell$$

were constructed with the wave functions of the core, Eq. (2), and the photoelectron wave functions $\epsilon\ell$. The corresponding photoionization cross sections $\sigma_{L_0S_0J_0}(EJ)$, which form a theoretical photoelectron spectrum, were calculated as described in Ref. [5]. Here, $L_0S_0J_0$ denotes the initial state by specifying the term of the main contribution to the initial state vector.

Ionization energies were calculated with the following equation:

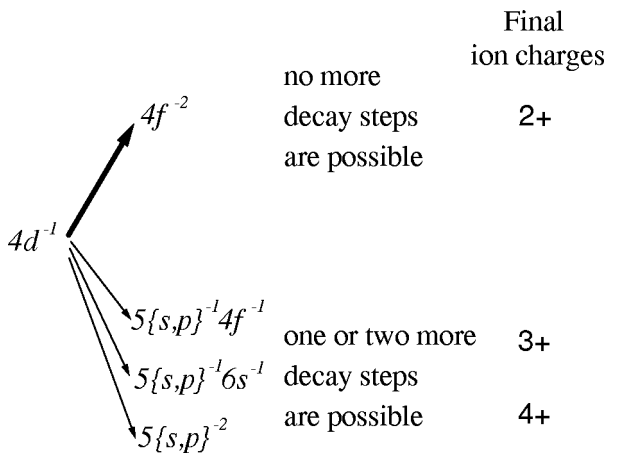


FIG. 2. Simplified scheme of cascade decay of the $4d$ vacancy in rare-earth atoms. When intense $4d-4f4f$ transitions are forbidden for the high-spin $4d^{-1}$ states, the yield of $2+$ photoions is suppressed.

$$\begin{aligned} I(L_0S_0J_0\rightarrow 4d^{-1}EJ) &= [E_{\mathrm{HFP}}(4d^{-1})+\Delta(EJ)] \\ &\quad -[E_{\mathrm{HFP}}(0)+\Delta(L_0S_0J_0)], \end{aligned} \tag{3}$$

where $E_{\mathrm{HFP}}(4d^{-1})$ and $E_{\mathrm{HFP}}(0)$ are mean Hartree-Fock-Pauli energies of the ionized and the ground-state configurations; $\Delta(EJ)$ and $\Delta(L_0S_0J_0)$ are the positions of $|EJ\rangle$ and $|L_0S_0J_0\rangle$ with respect to the center of gravity of the corresponding configuration. The calculated electron spectra of Ce, Pr, Nd, Sm, and Eu have been shifted by up to 1 eV in order to allow comparison with the corresponding experimental spectra.

In this work, the distributions of the high-spin states $^{2S_{\max}+1}L_J$ over the $|EJ\rangle$ states of the $4d^{-1}$ multiplets are investigated. The high-spin states are those states in which all the electron spins of the $4f$ (or $4f$ and $5d$) subshell and the spin of the $4d$ vacancy have the same orientation. Hence, $S_{\max}$ in $^{2S_{\max}+1}L_J$ is equal to $\frac{1}{2}(N_{4f}+N_{5d}+1)$, where $N$ is the subshell occupation number. To demonstrate the distribution of the high-spin states over the $4d^{-1}$ multiplet components, we calculated the values

$$\beta(EJ)=\sum_i \langle 4d^9 4f^n\gamma_i,L_i,S_{\max}J|EJ\rangle^2, \tag{4}$$

which represent the weight of the high-spin states $^{2S_{\max}+1}L_J$ in each $4d^{-1}$ multiplet component.

The $4d^{-1}$ states decay predominantly by Auger cascades, which lead to final ion charges of $2+$ to $5+$. As pointed out in Ref. [5], these cascades depend on the spin of the $4d^{-1}$ states, the decay of high-spin and low-spin ($S<S_{\max}$) states being quite different. This is due to the fact that intense super-Coster-Kronig $4d-4f4f$ transitions are forbidden for the high-spin states. For example, a high-spin state $4d^9 4f^n(n\leqslant 7)$, which has a spin $S_{\max}=\frac{1}{2}(n+1)$, cannot decay by $4d-4f4f$ transitions into $4d^{10}4f^{n-2}\epsilon\ell$ states, since the spin of these final states is only $S_{\max}=\frac{1}{2}(n-1)$. Similar considerations hold also for $4d-4f5d$ transitions in Ce and Gd. Figure 2 illustrates the formation of final ion charges for

different decay branches. If allowed, intense $4d-4f4f$ transitions are the principal producers of $2+$ ions, because $4f$ vacancies cannot decay further. Other first-step decay branches create the states with $5s$ and/or $5p$ vacancies, which can decay further leading to the formation of $3+$ and $4+$ ions. Therefore, if the initial $4d^{-1}$ state is a high-spin state, the yield of $2+$ ions will be low, since it results only from low-intensity $4d-4f6s$, $4d-6s6s$, and shake processes. For low-spin $4d^{-1}$ states, $4d-4f4f$ transitions are allowed and the yields of $2+$ and $3+$ ions should be of the same order of magnitude.

Each $|EJ\rangle$ state of the $4d^{-1}$ multiplet has specific contributions from both high-spin and low-spin states, and, therefore, behaves differently with respect to the formation of ions. We propose an approximate formula to calculate partial photoionization cross sections for the formation of ions of specific charges:

$$\sigma^{n+}_{L_0S_0J_0}(EJ)=\sigma_{L_0S_0J_0}(EJ)\times\{\beta(EJ)P^f(n+)+[1-\beta(EJ)]P^a(n+)\}. \tag{5}$$

Here, $\sigma_{L_0S_0J_0}(EJ)$ is the photoionization cross section, and $\beta(EJ)$ is determined by Eq. (4). $P^a(n+)$ and $P^f(n+)$ are the ion yields calculated with either allowed ($P^a$) or forbidden ($P^f$) $4d-4f4f$ transitions. The calculation of these values is described in Sec. III B. The sets of values of Eq. (5) represent the theoretical FIRE($n+$) spectra.

As was pointed out in Sec. II, under our experimental conditions (high-temperature atomic beams) there exists a noticeable probability of photoionizing atoms not only in their ground state, but also in thermally populated states. The population of various initial states $L_0S_0J_0$, calculated from the Boltzmann distributions, is presented in Table I. Only Eu, with a half-filled $4f$ subshell, has a well-separated ground state $^8S_{7/2}$ term. For all other elements, the thermal population of initial states is quite high. Thus, we have to compare the measured spectra with the superpositions of specific $L_0S_0J_0$ spectra weighted according to the thermal initial state population. In order to illustrate the effect of thermally populated initial states, we present in Fig. 3 the $4d$ photoelectron spectra of Nd calculated for the three lowest initial states $L_0S_0J_0$ [panels (a)–(c)], and the weighted superposition of those spectra [panel (d)]. In the case of Pm and Gd, the calculations were performed only for the ground states $^6H_{5/2}$ and $^9D_2$, respectively, since for these elements a comparison with our own experimental results was not possible.

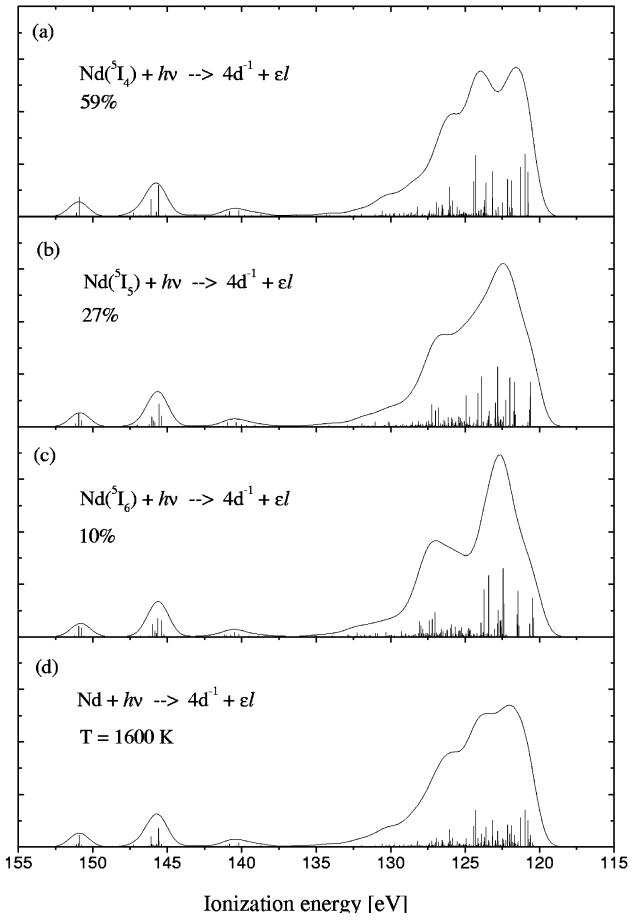


FIG. 3. Nd $4d$ photoelectron spectra. (a)–(c) Spectra calculated for separate initial $L_0S_0J_0$ terms; (d) superposition of $L_0S_0J_0$ spectra weighted according to the thermal population (see Table I). Spectra are convoluted with Gaussians having FWHM of 1.5 eV.

### B. Calculation of ion yields

Our calculations of ion yields are based on the straightforward construction of deexcitation trees in the configuration-average approximation. Since the method is described in detail elsewhere [17,18], only a brief description is given.

At each branching point (initial or intermediate configuration of a cascade), branching ratios are expressed through the total and partial Auger widths, while radiative branches are neglected. Partial widths for nonradiative $i-jk$ transitions are expressed in a factorized form, thus allowing one to separate the dependence on the occupation numbers of atomic subshells:

$$\Gamma_{ijk}=N_i^v N_{jk}^p \gamma_{ijk}. \tag{6}$$

Here $i,j,k$ denote the electron subshells involved in a transition, $N_i^v$ the number of vacancies in the subshell $i$, and $N_{jk}^p$ the number of possible pairs of the $j$ and $k$ subshell electrons that can participate in the transition. The reduced partial width per one pair of electrons $\gamma_{ijk}$ is a combination of Slater integrals and depends rather smoothly on the configuration of the decaying ion [17]. Equation (6) allows one to calculate nonradiative partial level widths for a great variety of intermediate configurations of a cascade and to include relaxation effects on nonradiative widths due to the dependence of $\gamma_{ijk}$ on the number of vacancies in the shells of an ion.

Our model includes monopole shake-off processes caused by the change of the core potential in the course of the development of a cascade. Shake-off probabilities are calculated in the sudden limit approximation [19]:

$$W_{nl}=N_{nl}[1-\langle nl(\text{init. conf.})|nl(\text{final conf.})\rangle^2]. \tag{7}$$

$W_{nl}$ is the probability for one electron to be shaken off from subshell $nl$ due to the sudden change of the configuration of the core, and $N_{nl}$ the occupation number of the $nl$ subshell.

TABLE II. Relative ion yields produced by $4d^{-1}$ cascades calculated with allowed $P^a$ or forbidden $P^f$ s-CK $4d-4f4f$ transitions.

| Ion | Ce | | Pr | | Nd | | Pm | | Sm | | Eu | | Gd | |
|---|---|---|---|---|---|---|---|---|---|---|---|---|---|---|
| charge | $P^a$ | $P^{f\text{a}}$ | $P^a$ | $P^f$ | $P^a$ | $P^f$ | $P^a$ | $P^f$ | $P^a$ | $P^f$ | $P^a$ | $P^f$ | $P^a$ | $P^{f\text{b}}$ |
| 2+ | 0.081 | 0.021 | 0.309 | 0.026 | 0.395 | 0.026 | 0.460 | 0.027 | 0.504 | 0.027 | 0.613 | 0.025 | 0.498 | 0.028 |
| 3+ | 0.577 | 0.614 | 0.644 | 0.918 | 0.563 | 0.920 | 0.507 | 0.938 | 0.451 | 0.905 | 0.359 | 0.897 | 0.366 | 0.625 |
| 4+ | 0.319 | 0.340 | 0.047 | 0.056 | 0.042 | 0.054 | 0.033 | 0.035 | 0.045 | 0.068 | 0.028 | 0.078 | 0.133 | 0.342 |
| 5+ | 0.023 | 0.024 | | | | | | | | | | | 0.003 | 0.005 |

[a] $4d-4f5d$ transitions are forbidden.

[b] Both $4d-4f4f$ and $4d-4f5d$ transitions are forbidden.

We express the overlap integrals in Eq. (7) in terms of mean Hartree-Fock radii of the $nl$ subshell in the initial and final configurations. Atomic orbital mean radii depend very smoothly on the atomic configuration and can be calculated with simple interpolation formulas for any intermediate configuration of a cascade as described in Ref. [18].

The multiplets of the initial and final configurations for some transitions in a cascade may overlap. In those cases, some of the transitions between the states of the multiplets are energetically forbidden, and the configuration-average widths, Eq. (6), should be decreased. On the other hand, some transitions between some states of overlapping multiplets are allowed even if the mean energy of the initial configuration is less than that of the final configuration. We account for those partially forbidden transitions by simulating the multiplets with Gaussian frequency functions. Variances of the multiplet distributions for any configuration can be expressed in terms of minimal sums and occupation numbers of the electron subshells [20].

Thorough analysis of deexcitation trees of the $4d^{-1}$ cascades in rare earths showed that they are very sensitive to the energy positions of the ionic levels. For this reason we used total Hartree-Fock-Pauli energies of cascade configurations for the positioning of the ionic levels.

For each element, the ion yields were calculated in two different ways. The ion yields $P^a(n+)$ are obtained by taking into account all the branches in the deexcitation trees ($4d-4f4f$ transitions are allowed). On the other hand, the ion yields $P^f(n+)$, for which $4d-4f4f$ transitions are forbidden, are obtained by neglecting the $4d-4f4f$ and $4d-4f5d$ decay branches in the construction of the deexcitation trees.

The calculated ion yields are listed in Table II. When the $4d-4f4f$ and $4d-4f5d$ transitions are forbidden, the yields of 2+ ions decrease drastically. This effect becomes more pronounced for heavier atoms, because with the increase of the number of $4f$ electrons the relative strength of the $4d-4f4f$ decay branch becomes greater. The yields of 5+ ions are negligible for Pr to Eu, while noticeable 5+ yields were calculated for Ce and Gd, which have an additional $5d$ electron. Greater 2+ abundance in Ce is connected with the greater relative importance of the $4d-5s5s$ decay branch.

## IV. RESULTS AND DISCUSSION

Measured and calculated $4d$ photoelectron spectra of Ce to Gd are presented in Figs. 4 and 5. The measured spectra are shown with dots and error bars. For better comparison with the calculated spectra, the continuous background has been subtracted. This continuous background is due to direct double photoionization and double Auger processes, where two electrons are emitted simultaneously. The theoretical spectra were calculated as described in Sec. III A, whereby the thermal population of the initial states with respect to the experimental conditions (see Table I) was taken into account. Each vertical bar represents the photoionization cross section for a specific multiplet component. Solid curves are obtained by convoluting the bar spectra with Gaussians of fixed full width at half-maximum (FWHM) corresponding to the experimental resolution of the electron analyzer and the bandwidth of the monochromator. The distributions of the high-spin states $^{2S_{\max}+1}L_J$ over the $4d^{-1}$ multiplets are displayed as dotted curves and were obtained by weighting the cross sections of the multiplet components by the fraction of high-spin states [see Eq. (4)].

The photoelectron spectra show a large multiplet splitting of about 30 eV due to the strong $4d-4f$ electrostatic interaction. Until now, experimental data have been available only for the low ionization energy part. The overall agreement of theory and experiment in this region is good. Since in the low ionization energy region the natural lifetime widths of the $4d^{-1}$ states are of the order of 0.1 eV [7,8,11], the broadening of the spectral components is mainly due to the experimental resolution. This does not hold for the high ionization energy region, where the natural width is about 2 eV [11]. Therefore, in the high ionization energy region the experimental spectra are expected to be broader than the corresponding calculated spectra depicted in Figs. 4 and 5.

The $4d^{-1}$ states essentially maintain their atomic character in solids. However, for the comparison of atomic and solid state data, different $4f^n$ occupation numbers in atoms and in metals should be considered [21,22]: Ce($4f5d$), Eu($4f^7$), and Gd($4f^75d$) maintain their atomic $4f$ occupancy in metals, while for Pr($4f^3$), Nd($4f^4$), Pm($4f^5$), and Sm($4f^6$) the $4f^n$ occupation number decreases by 1 in the solid state. Therefore, Ce and Gd, because of the additional $5d$ electron, and Sm have no solid state counterparts. On the other hand, our calculations on radioactive Pm correspond to studies of metallic Sm. A comparison of our results for atomic Pm($4f^56s^2$) and Eu($4f^76s^2$) with those of Ref. [11] on $Sm^{3+}(4f^5)$ and $Gd^{3+}(4f^7)$ in metals show close agreement between the shapes of the measured and calculated spectra. The $4d$ photoelectron spectrum of metallic Nd measured by Platau [23] is quite similar to our spectrum of atomic Pr. However, the extent of the splitting within multiplets in atoms and in the corresponding ions within metals

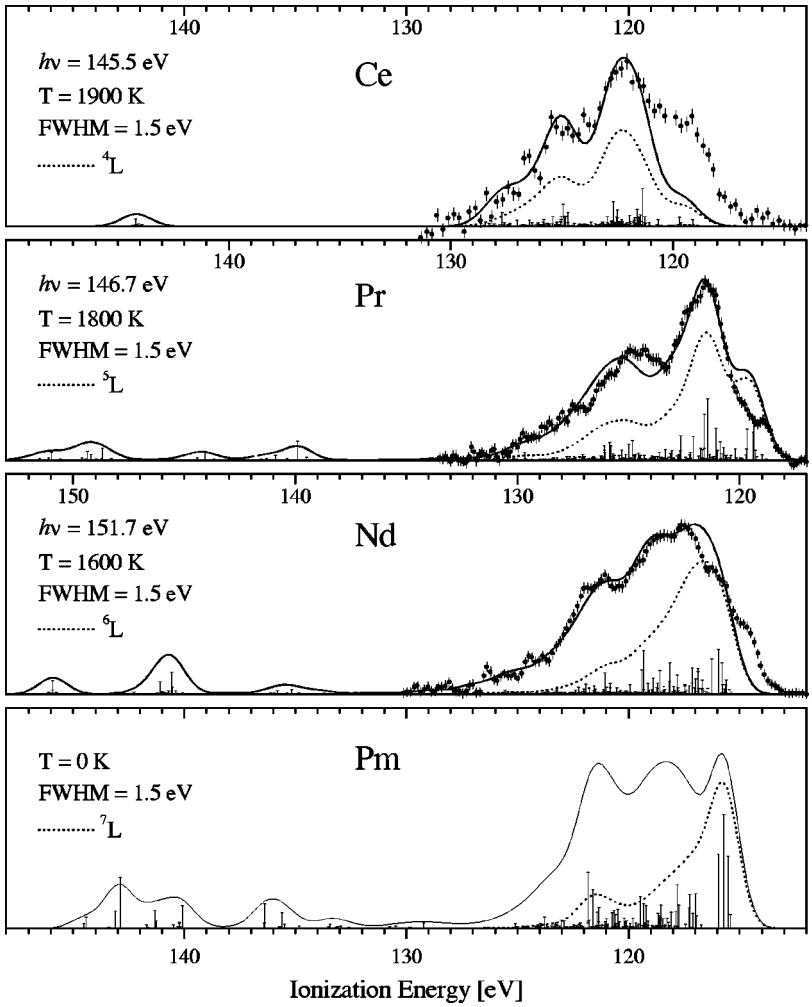


FIG. 4. Measured and calculated $4d$ photoelectron spectra of Ce, Pr, Nd, and Pm. Dots with error bars (●●●), experimental spectra; vertical bars (|), photoionization cross section calculated for each multiplet component; solid curves (—), theoretical spectra obtained by convolution of the bar spectra with Gaussians of fixed FWHM; dotted curves (···), theoretical spectra weighted by the fraction of high-spin states $^{2S_{\max}+1}L$.

is somewhat different due to the different magnitudes of the electron-electron interaction. An additional reason for slight differences between atomic and solid state spectra results from the thermal population of the initial states in atomic-beam experiments (see Fig. 3 and Table I). The comparison of our atomic calculations with the solid state measurements shows that the nature of the $4d$ vacancy in $4f$ metals is essentially of atomic character. Therefore, the accurate description of $4d^{-1}$ multiplets in both atomic and metallic rare earths is only possible by means of thorough consideration of direct and exchange electron-electron interaction.

The $4d^{-1}$ multiplets of the rare-earth atoms investigated consist of a low ionization energy and a high ionization energy region. The low ionization energy region of the elements Ce to Pm is characterized by a broad structure of varying shape (Fig. 4), while for Sm to Gd this region is divided into two peaks (Fig. 5). According to our calculations, the low ionization energy structures are represented by high-spin states $^{2S_{\max}+1}L_J$ and low-spin states $^{2S_{\max}-1}L_J$. These states originate from the interaction of the $4d$ vacancy with the $4f^n$ states of the largest and the second-largest multiplicities, respectively. The dominant contribution to the high ionization energy region is provided by low-spin states $^{2S_{\max}-1}L_J$, which come from antiparallel coupling of the electron spin of the $4d$ vacancy and the energetically lowest $4f^n$ state of the largest multiplicity.

As mentioned in Sec. I, contradictory assignments exist for the localization of high-spin states within the low ionization energy part of the $4d^{-1}$ multiplets. To study the distribution of high-spin states $^{2S_{\max}+1}L_J$ over the $4d^{-1}$ multiplets, each component of the calculated photoelectron spectra has been weighted with the fraction of high-spin states $\beta(EJ)$ for that component [see Eq. (4)]. The results are shown in Figs. 4 and 5 as dotted curves. As can be seen from Fig. 4, the high-spin states tend to become more and more concentrated at lower ionization energies when going from Ce to Pm. Finally, in the case of Sm, Eu, and Gd the high-spin states are localized mainly within the peak at lower ionization energy, while the accompanying peak has predominantly low-spin character (Fig. 5).

Such behavior of the high-spin state distributions results from the relative positioning of $^{n+1}L_J$ and $^{n-1}L_J$ states of the $4f^n$ subshells. In Pr, Nd, and Pm, the largest-multiplicity states $^{n+1}L_J$ are spread over an interval of about 3 eV and overlap considerably with $^{n-1}L_J$ states. Better localization

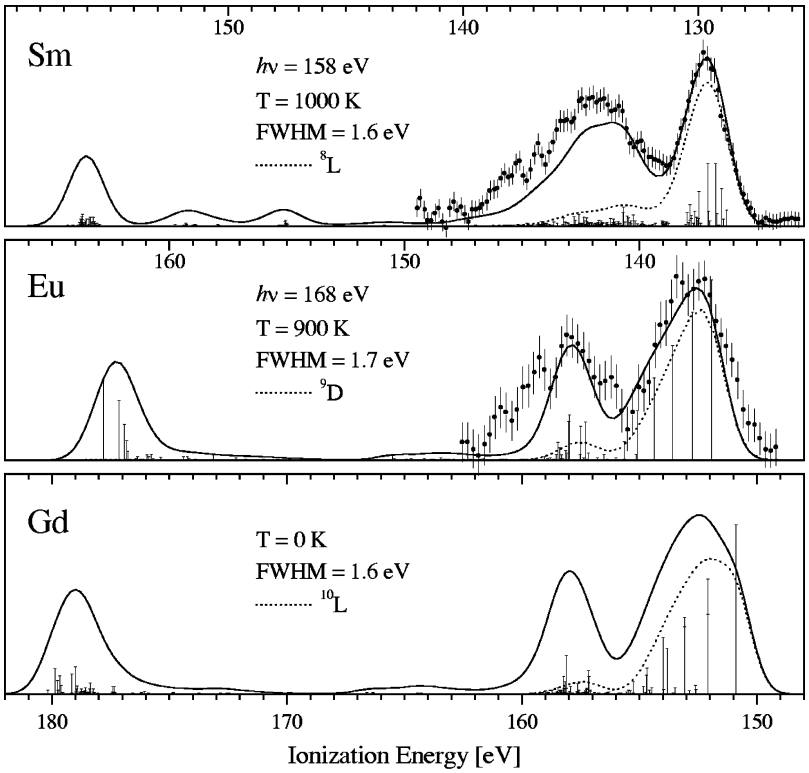


FIG. 5. Measured and calculated $4d$ photoelectron spectra of Sm, Eu, and Gd. Dots with error bars (●●●), experimental spectra; vertical bars (|), photoionization cross section calculated for each multiplet component; solid curves (—), theoretical spectra obtained by convolution of the bar spectra with Gaussians of fixed FWHM; dotted curves (···), theoretical spectra weighted by the fraction of high-spin states $^{2S_{\max}+1}L$.

of the high-spin states in Pm is due to the fact that its $4f^5$ subshell has only three $^6L$ terms, while the $4f$ subshells of Pr and Nd have five terms with the largest multiplicity ($^4L$ and $^5L$, respectively). In Sm($4f^6$), Eu($4f^7$), and Gd($4f^7 5d^1$), the $4f$ subshells have only one largest multiplicity term, i.e., $4f^6(^7F)$ and $4f^7(^8S)$. Furthermore, these terms are separated energetically from the corresponding $^5L$ and $^6L$ terms, thus forming a well-resolved low ionization energy group of the $4d^{-1}$ components that has predominantly high-spin character. High-spin states in Ce arise from the coupling of the $4f$ and the $5d$ electron to $^3L$ states and demonstrate almost no localization within the low ionization energy region.

The theoretical results for the distribution of high-spin states over the $4d^{-1}$ multiplet components described above need to be verified experimentally. Photoelectron spectroscopy is an ideal tool to investigate the strength of photoionization cross sections. However, spin-sensitive methods are necessary to obtain information about the spin character of core-hole states. Magnetic dichroism in the photoemission as well as angle and spin resolved photoelectron spectroscopy are examples of spin-sensitive methods which have been developed recently. FIRE spectroscopy on rare-earth atoms is another example of a spin-sensitive technique. Here, the information about the spin is provided by the decay process following the creation of a $4d$ core-hole.

Measured and calculated photoelectron and FIRE($n+$) spectra ($n=2,3,4$) of the low ionization energy region are depicted in Figs. 6–10 for Eu, Sm, Nd, Pr, and Ce. As $1+$ ions were not observed within the error bars, radiative decays are negligible. A FIRE($n+$) spectrum represents that contribution of electrons to the electron spectrum that is connected with photoionization processes ending up in an $n+$ final ion-charge state. Experimental spectra are shown with background, unlike in Figs. 4 and 5, where background has been subtracted. The data points of the experimental FIRE spectra were calculated with Eq. (1), and the error bars result from the determination of the correlation probabilities. The solid curves representing the experimental spectra were obtained in two different ways. For Eu, Sm, and Pr, fit curves consisting of a superposition of Gaussian profiles were used. Only the amplitudes and not the positions and the widths of the Gaussian profiles as obtained from the fit to the corresponding photoelectron spectrum were varied for the fits to the FIRE spectra. In the case of Ce and Nd, the solid curves were obtained by smoothing the data points. The upper panels of the experimental results show the measured photoelectron spectra as data points with error bars and the sum of the FIRE spectra as a solid line. The calculated photoelectron spectra and distributions of high-spin states displayed in the upper panel of the theoretical results are identical with those in Figs. 4 and 5. The FIRE spectra were calculated with Eq. (5). As in the case of the photoelectron spectra, the population of the initial states was included in the FIRE spectra and the Gaussian convolutions were performed.

As discussed in Sec. III A, the most severe variation of spectral shapes is expected in the FIRE($2+$) spectra, since the most pronounced changes due to forbidden $4d-4f4f$

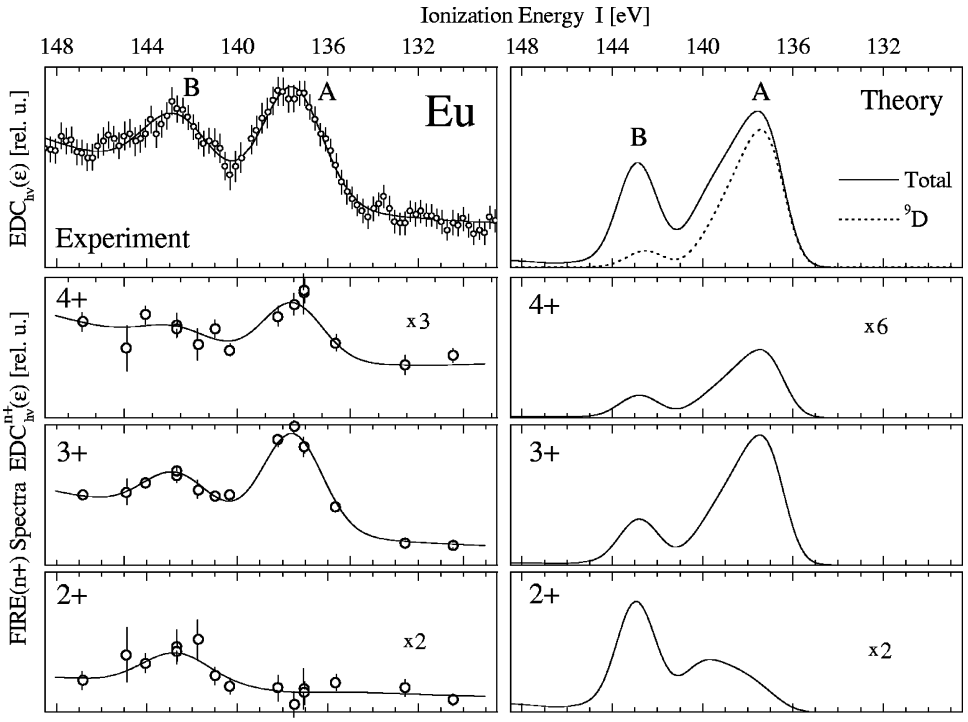


FIG. 6. Measured and calculated $4d$ photoelectron and FIRE($n+$) spectra of Eu in the low ionization energy region.

transitions occur in the $2+$ ion yields, as can be seen in Table II. The relative intensities should be drastically suppressed in those regions of the FIRE($2+$) spectra that represent the $4d^{-1}$ states of predominantly high-spin character. The effect is more pronounced in the spectra of those atoms where the high-spin states are well localized, as in Eu (see Fig. 6), where the $4d$ photoelectron spectrum has a two-peak structure (peaks are labeled $A$ and $B$). Peak $A$ is strongly suppressed in the Eu FIRE($2+$) spectrum in contrast to peak $B$. Therefore, it is evident that peak $A$ is mainly composed of the high-spin $^9D$ states, while peak $B$ represents predominantly $4d^9(^2D)4f^7(^6L)^7D$ states. This assignment is in

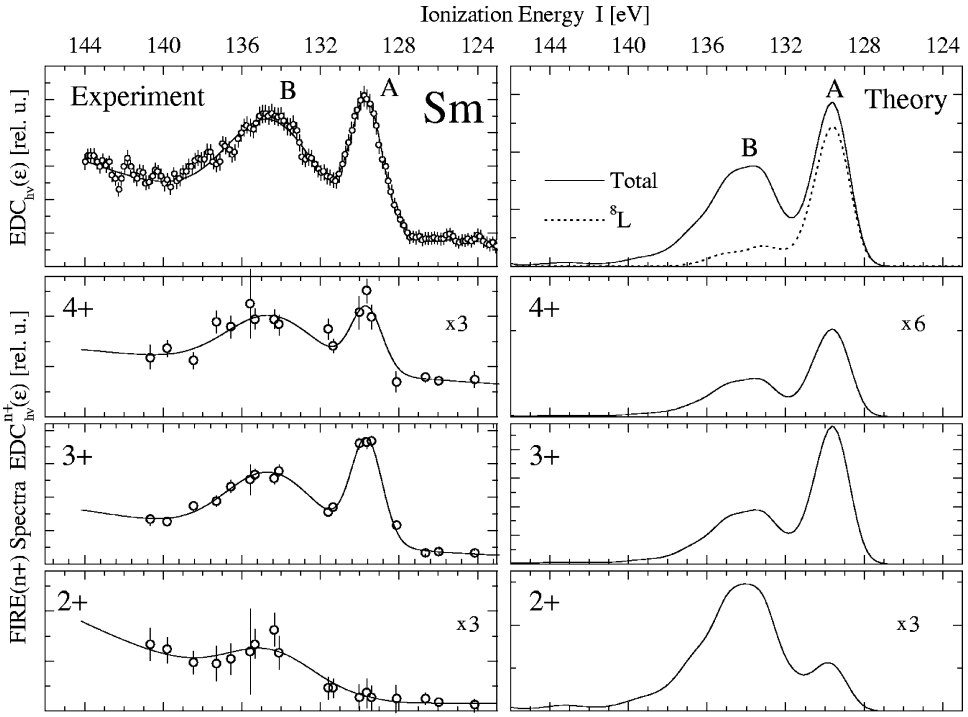


FIG. 7. Measured and calculated $4d$ photoelectron and FIRE($n+$) spectra of Sm in the low ionization energy region.

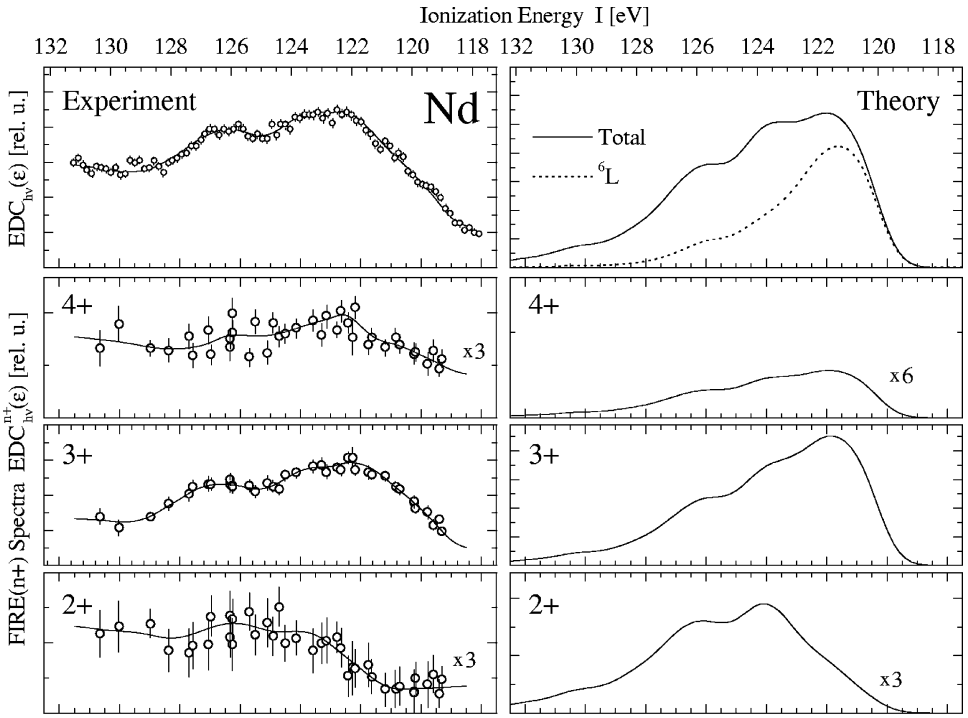


FIG. 8. Measured and calculated $4d$ photoelectron and FIRE($n+$) spectra of Nd in the low ionization energy region.

agreement with those given by Lademan *et al.* [8] and van der Laan *et al.* [7] based on magnetic circular dichroism and spin-resolved studies in the $4d$ photoemission of metallic Gd. Similarities to Eu can be found in atomic Cr with its half-filled $3d$ subshell. The $3p$ photoelectron spectrum of atomic Cr also shows a two-peak structure at the low ionization energy region of the $3p^{-1}$ multiplet. Having studied the dichroism in the $3p$ photoionization of polarized Cr atoms, von dem Borne *et al.* [12] assigned the peaks at lower ionization energy to high-spin states ($^8P$) and the neighboring peaks with higher ionization energy to low-spin states ($^6P$).

The FIRE($2+$) spectrum of Sm depicted in Fig. 7 looks strikingly similar to that of Eu with peak $A$ again strongly suppressed. It implies that peak $A$ is again related to high-spin states ($^8L$), while peak $B$ is mainly formed by low spin states ($^6L$). Although we have not yet measured FIRE spec-

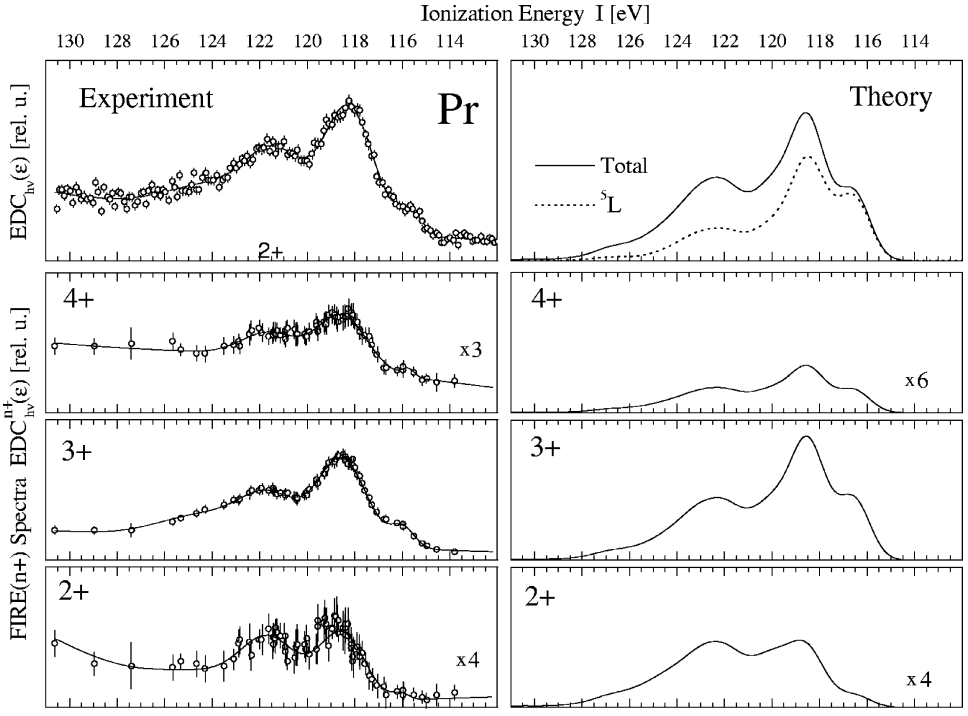


FIG. 9. Measured and calculated $4d$ photoelectron and FIRE($n+$) spectra of Pr in the low ionization energy region.

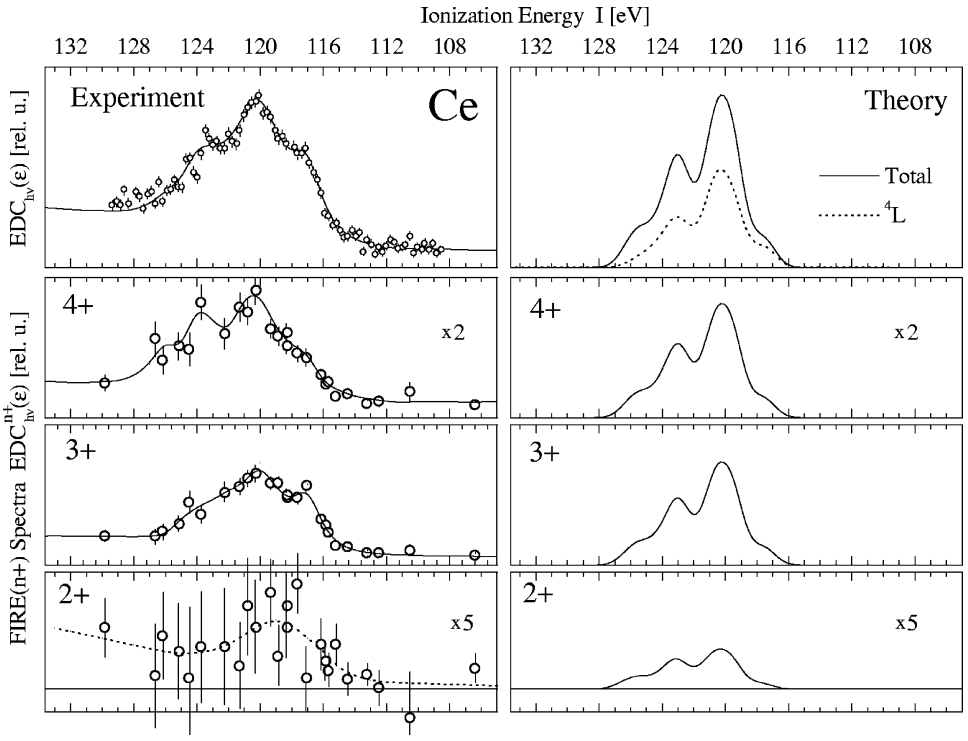


FIG. 10. Measured and calculated $4d$ photoelectron and FIRE($n+$) spectra of Ce in the low ionization energy region.

tra of Gd, similar division into a predominantly high-spin ($^{10}L$) and a low-spin ($^{8}L$) peak as predicted by the theory (see Fig. 5) is supported by the FIRE experiments on Eu and Sm. The only difference between Eu and Gd is the presence of an additional $5d$ electron in Gd, whose interaction with $4d$ and $4f$ electrons is weaker than the $4d-4f$ and $4f-4f$ interactions determining the main features of the $4d^{-1}$ multiplets.

In the case of the $4d$ spectra of Nd and Pr, a division into high-spin and low-spin peaks is not possible, as can be seen from the calculated spectra of Figs. 8 and 9 (upper panels, dotted curves). The high-spin states are distributed over the whole low ionization energy region. Nevertheless, there exists a distinct asymmetry in the distributions of high-spin states: their weight grows upon moving to the lower ionization energy side of the spectra. This asymmetry again leads to significant changes in the shapes of the calculated FIRE(2+) spectra. These changes are reproduced well in the measured FIRE(2+) spectra of Nd and Pr.

In the case of Ce (Fig. 10), the high-spin states do not demonstrate any localization or asymmetry within the $4d^{-1}$ multiplet, where almost all the components have approximately equal fraction of high-spin and low-spin states. For this reason, only slight changes in the shapes of the FIRE spectra are predicted by theory. Since the 2+ ion yield in Ce is very weak as compared with the other atoms (see Table II), it is hardly possible to deduce the actual shape of the Ce FIRE(2+) spectrum from the experimental data. However, as can be seen from the lower panels of Fig. 10, the extent of the experimental FIRE(2+) structure and its integral relative intensity are comparable with the respective theoretical values.

The spectral shapes of the FIRE(3+) and FIRE(4+) spectra of Pr to Eu differ only slightly from the shapes of the photoelectron spectra. The multiplet components with high-spin character, which are suppressed in the FIRE(2+) spectra, are enhanced in the FIRE(3+) and FIRE(4+) spectra. For Sm and Eu, where the high-spin states are well localized in the spectra (peak $A$), the 3+ and 4+ ion yields increase differently (see Table II). The ratio of forbidden to allowed $4d-4f4f$ transitions for the 3+ ion yield of Eu is $P^f(3+)/P^a(3+)=2.4$, whereas the ratio for the 4+ ion yield is $P^f(4+)/P^a(4+)=2.8$. Therefore, the relative intensity of the high-spin peak $A$ should be higher in the FIRE(4+) spectrum. This is supported experimentally, as can be seen in Fig. 6. For Sm, the situation is different: here we have $P^f(3+)/P^a(3+)=2.0$ and $P^f(4+)/P^a(4+)=1.5$, and so we expect that the relative intensity of peak $A$ should be higher in the Sm FIRE(3+) spectrum. This is confirmed by the experimental data depicted in Fig. 7. Of course, a simple qualitative analysis of this kind is not applicable in the case of Nd and Pr, which have widely spread high-spin states. However, the shapes of the experimental and the theoretical FIRE spectra (Figs. 8 and 9) show similar behavior.

It should be noted that a disagreement exists in the overall relative intensities of the FIRE spectra of Pr to Eu. For these elements, the calculated relative intensities of the FIRE(4+) spectra are smaller by roughly a factor of 2 than the corresponding experimental quantities [note that the FIRE(2+) and FIRE(4+) spectra are stretched along the vertical axes by the factors specified in Figs. 6–10]. On the other hand, the calculated and measured relative intensities of the FIRE spectra agree much better in the case of Ce (Fig. 10). The discrepancy in the case of Pr, Nd, Sm, and Eu might be explained by the fact that we took the initial configurations of the cascades to be $4f^n6s^2$, despite the fact that a noticeable $6s-5d$ configuration interaction should also be present.

As can be seen from the calculations of the ion yields in Ce and Gd, the presence of the $5d$ electron substantially increases the yield of $4+$ ions. Therefore, going beyond the one-configuration approximation in the calculations of both multiplet structures and ion yields might improve the agreement with the experiment.

In conclusion, the results discussed above establish FIRE spectroscopy as a spin-sensitive method that allows one to study the compositions of $4d^{-1}$ multiplet states of rare-earth atoms. Its sensitivity is based on the asymmetry of the decay processes for high-spin and low-spin states of the $4d^{-1}$ multiplet components. Due to the strong $4d-4f$ electrostatic interaction, the $4d^{-1}$ multiplets in rare earths extend over an energy range of about 30 eV. The low ionization energy region consists of both high-spin and low-spin states. For Ce, the high-spin states are completely spread over the low ionization energy region, whereas the high-spin states become more and more localized as the atomic number increases (Pr to Pm). The low ionization energy region of Sm, Eu, and Gd is split into two peaks, which can be assigned to high-spin and low-spin states. The dependence of the FIRE$(n+)$ spectra on the final ion charge can be understood within a theoretical model based on forbidden $4d-4f4f$ super-Coster-Kronig decays for high-spin $4d^9 4f^n (n \leqslant 7)$ states. For the calculations of the theoretical FIRE spectra, we combine calculations of the $4d^{-1}$ multiplets in the one-configuration approximation with calculations of ion yields in the configuration-average approximation.

## ACKNOWLEDGMENTS

The authors are grateful to Professor V. L. Sukhorukov for bringing to their attention the possibility of the theoretical calculation of the FIRE spectra, and for the discussion of the results. They are also grateful to Dr. I. D. Petrov for providing the computer code for the calculation of multiplet structures in atoms with up to three open shells. One of the authors (A.G.K.) is thankful to his colleagues at the Technische Universität Berlin for the invitation to work on this problem, and for their hospitality during his stay in Berlin. The financial support of the Deutsche Forschungsgemeinschaft (Project Nos. 436RUS and Zi183/11-2) is gratefully acknowledged. Special thanks are expressed to the staff at BESSY for their continuous assistance.

[1] M. Richter, J. Electron Spectrosc. Relat. Phenom. **76**, 21 (1995).
[2] T. Luhmann, Ch. Gerth, M. Martins, M. Richter, and P. Zimmermann, Phys. Rev. Lett. **76**, 4320 (1996).
[3] T. Luhmann, Rev. Sci. Instrum. **68**, 2347 (1997).
[4] T. Luhmann, Ch. Gerth, M. Groen, M. Martins, B. Obst, M. Richter, and P. Zimmermann, Phys. Rev. A **57**, 282 (1998).
[5] A. G. Kochur, V. L. Sukhorukov, and I. D. Petrov, J. Phys. B **39**, 4565 (1996).
[6] V. F. Demkhin, S. A. Yavna, Yu. I. Bairachnyi, and V. L. Sukhorukov, J. Struct. Chem. **18**, 513 (1977) [translated from Zh. Strukt. Khim. **18**, 644 (1977)].
[7] G. van der Laan, E. Arenholz, E. Navas, A. Bauer, and G. Kaindl, Phys. Rev. B **53**, R5998 (1996).
[8] W. J. Lademan, A. K. See, L. E. Klebanoff, and G. van der Laan, Phys. Rev. B **54**, 17 191 (1996).
[9] M. Richter, M. Meyer, M. Pahler, T. Prescher, E. v. Raven, B. Sonntag, and H. E. Wetzel, Phys. Rev. A **39**, 5666 (1989).
[10] M. Richter, M. Meyer, M. Pahler, T. Prescher, E. v. Raven, B. Sonntag, and H. E. Wetzel, Phys. Rev. A **40**, 7007 (1989).
[11] H. Ogasawara, A. Kotani, and B. T. Thole, Phys. Rev. B **50**, 12 332 (1994).
[12] A. von dem Borne, T. Dohrmann, A. Verweyen, B. Sonntag, K. Godehusen, and P. Zimmermann, Phys. Rev. Lett. **78**, 4019 (1997).
[13] K. J. Ross and B. Sonntag, Rev. Sci. Instrum. **66**, 4409 (1995).
[14] W. Wiley and I. McLaren, Rev. Sci. Instrum. **26**, 1150 (1955).
[15] A. P. Jucys and A. J. Savukinas, *Mathematical Foundation of the Atomic Theory* (Mintis, Vilnius, 1973).
[16] I. Lindgren and J. Morrison, *Atomic Many-body Theory*, 2nd ed. (Springer, Berlin, 1986).
[17] A. G. Kochur, A. I. Dudenko, V. L. Sukhorukov, and I. D. Petrov, J. Phys. B **27**, 2157 (1994).
[18] A. G. Kochur, V. L. Sukhorukov, I. D. Petrov, and Ph. V. Demekhin, J. Phys. B **28**, 387 (1995).
[19] V. P. Sachenko and V. F. Demekhin, Zh. Eksp. Teor. Fiz. **49**, 765 (1965) [Sov. Phys. JETP **22**, 532 (1966)].
[20] R. Karaziya, *Sums of Atomic Quantities and Mean Characteristics of Spectra* (Mokslas, Vilnius, 1991).
[21] J. F. Herbst, Phys. Rev. B **28**, 4204 (1983).
[22] M. Richter, T. Prescher, M. Meyer, E. v. Raven, B. Sonntag, H. E. Wetzel, and S. Aksela, Phys. Rev. B **38**, 1763 (1988).
[23] A. Platau, Ph.D. thesis, Linköping University, Sweden (1982).
[24] W. C. Martin, R. Zalubas, and L. Hagan, *Atomic Energy Levels—The Rare-Earth Elements*, U.S. Department of Commerce, National Technical Information Service PB-282 067, April, 1978 (U.S. GPO, Washington, D.C., 1978).